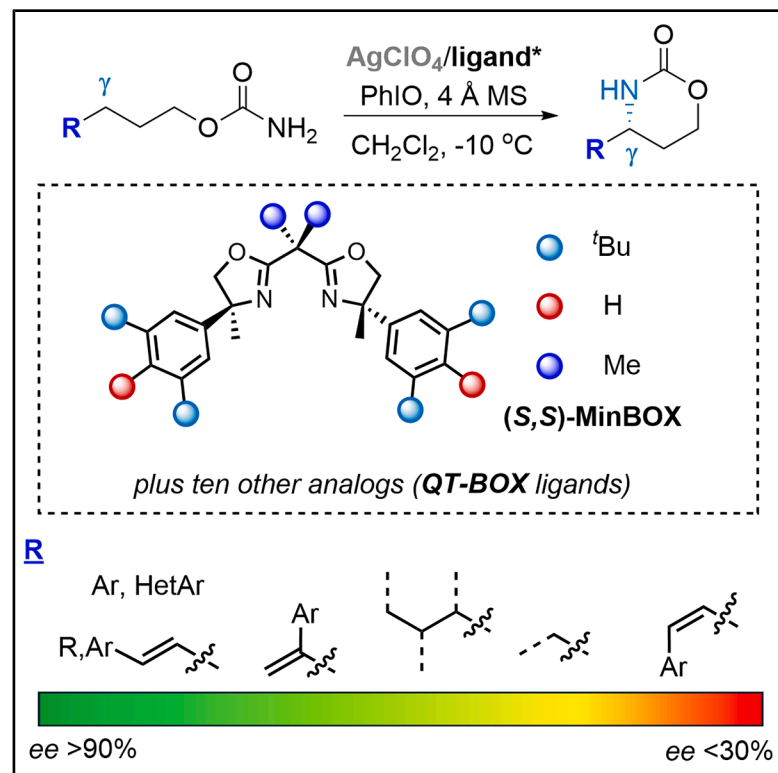# Chem Catalysis

Modular silver catalysts to elucidate the role of non-covalent interactions in asymmetric C−H amidation reactions

Graphical abstract

Authors

Emily Z. Schroeder, Jed H. Kim, Yue Fu, Wentan Liu, Peng Liu, Jennifer M. Schomaker

Correspondence

pengliu@pitt.edu (P.L.), schomakerj@chem.wisc.edu (J.M.S.)

In brief

New modular ligands that support asymmetric Ag-catalyzed nitrene transfer into benzylic, allylic, and alkyl C–H bonds with high enantioselectivity (ee) are reported. Computational studies to shed insight into the key interactions dictating ee are presented. This work enables ready access to valuable amine synthetic building blocks important to drugs and bioactive molecules.

Highlights

- Silver catalysts for asymmetric amidation of diverse C−H bonds are reported

- Introduction of a modular platform for synthesis for new QT-BOX ligands

- Computations to support key interactions that influence enantioselectivity

- Application to a short synthesis of dapoxetine

9 INDUSTRY, INNOVATION AND INFRASTRUCTURE

CellPress

Article

Modular silver catalysts to elucidate the role of non-covalent interactions in asymmetric C−H amidation reactions

Emily Z. Schroeder,[1,3] Jed H. Kim,[1,3] Yue Fu,[2,3] Wentan Liu,[1] Peng Liu,[2,*] and Jennifer M. Schomaker[1,4,*]

[1]Department of Chemistry, University of Wisconsin–Madison, Madison, WI 53706, USA
[2]Department of Chemistry, University of Pittsburgh, 219 Parkman Avenue, Pittsburgh, PA 15260, USA
[3]These authors contributed equally
[4]Lead contact
*Correspondence: pengliu@pitt.edu (P.L.), schomakerj@chem.wisc.edu (J.M.S.)
https://doi.org/10.1016/j.checat.2025.101388

THE BIGGER PICTURE The chemo-, site-, and enantioselective formation of C–N bonds from C–H bonds via transition metal-catalyzed nitrene transfer is an attractive strategy to transform hydrocarbons into useful amine building blocks. The lack of inexpensive chemocatalysts for the asymmetric amidation of diverse C−H bonds remains an ongoing challenge in the field of C−H functionalization, despite the potential for such tools to greatly streamline the syntheses of valuable bioactive amines. In this work, we report a modular platform for the design of new bis(oxazoline) ligands bearing a quaternary stereocenter (QT-BOX). These ligands support Ag-catalyzed asymmetric nitrene transfers of benzylic, allylic, and unactivated C−H bonds to give products in high yields and good to excellent enantioselectivities. Computational studies were conducted to highlight the key non-covalent interactions in the transition state that govern the enantioselectivity.

SUMMARY

Chiral, non-racemic amines and aminoalcohols are common structural motifs in bioactive molecules. Asymmetric nitrene transfer offers a powerful approach to prepare enantioenriched amines directly from abundant C–H bonds; however, the development of general, cost-effective catalysts supported by easily tunable ligands remains a significant challenge. Herein, we report that Ag salts coordinated with unique bis(oxazoline) ligands catalyze site- and enantioselective nitrene transfer into benzylic, allylic, and unactivated C–H bonds of carbamate esters. This method provides 1,3-aminoalcohols in high yields with enantiomeric excess (*ee*) of up to 98%. Computations were used to rationalize key features influencing the observed stereochemical outcomes. Analysis of the enantiodetermining transition states revealed that high *ee* arises from a preferred square-planar geometry at the silver nitrene and stabilizing C–H/π interactions between the ligand and substrate. These features enable broad substrate scope and high chemo-, site-, and enantioselectivity in Ag-catalyzed C–H bond amidations via nitrene transfer.

INTRODUCTION

The transformation of C–H bonds into new C–N bonds is a powerful method for the synthesis of valuable amine building blocks that occur frequently in nitrogen-containing natural products and pharmaceuticals.[1,2] Transition metal-catalyzed nitrene transfer (NT) is a popular strategy to streamline access to these important compounds by facilitating direct C–H to C–N bond amidations. However, achieving predictable control over asymmetric NT events can be challenging using convenient sulfamate nitrene precursors. In particular, there is a lack of inexpensive chemocatalysts supported by modular and readily tunable ligands for the preparation of synthetically useful 1,3-aminoalcohols in an asymmetric manner.[3–5]

Enantioselective amidations of benzylic, allylic, and unactivated C–H bonds with a variety of nitrene precursors have been reported to form nitrogen-containing heterocycles and acyclic derivatives that include γ-lactams,[6,7] sulfamides,[8–11] sulfamates,[12–14] diamines,[9] and amino alcohols.[13–16] The γ-aminoarylpropanols and β-aminoarylethanols, accessible by ring opening of cyclic sulfamates or carbamates following the NT event, are particularly attractive targets, as they are found in diverse bioactive molecules, including dapoxetine,[17] the anticancer candidate capivasertib,[18] and CB1 inverse agonists for the potential treatment of obesity (Figure 1), among others.[19] In addition, the alcohol handle is easily elaborated into other useful enantioenriched amine scaffolds. Despite the utility of 1,2- and

1,3-aminoalcohols, asymmetric NT methods for their formation that display broad scope are scarce.

Most previous reports of asymmetric C–H bond amidations to yield 1,2- and 1,3-aminoalcohols utilize sulfamates and pre-oxidized carbamates as nitrene precursors (Scheme 1A), often with precious metal catalysts based on Rh, Ru, and Ir. For example, in the case of sulfamates as nitrene precursors, Du Bois found that the electronics of the aryl group impacted the *ee* of asymmetric benzylic C–H amidations catalyzed by dinu-clear Rh complexes[13]; the alkene geometry also played a role in the *ee* of the allylic amidation. Blakey's Ru(pyBOX) catalyst was less sensitive to arene electronics in terms of *ee*, but, in contrast to Rh$_2$(S-NAP)$_4$, (Z)-alkenes gave lower *ee* than (E)-al-kenes.[14] Davies and Meggers employed pre-oxidized carba-mate-derived nitrene precursors with asymmetric Rh and Ru catalysts to give the five-membered heterocyclic products, but these were also limited in scope.[15,16] While progress continues to be made in understanding how substrate effects impact the *ee* of NT, it is still not well understood, making it challenging to rationally design catalysts that furnish high *ee* when diverse car-bamates are employed as nitrene precursors.

We developed a new bis(oxazoline) ligand ((S,S)-Min-BOX, Scheme 1B, R = Me, R^1 = 3,5-di-*t*-Bu, R^2 = Me) for Ag-catalyzed propargylic C–H bond amidation that delivers propargylic amines in high *ee*.[20–22] Key features of the ligand include a fully substituted stereocenter on the oxazoline ring and significant steric bulk in the form of 3,5-*tert*-Bu groups on the aryl ring. Com-putations highlighted the importance of the rigidity of the alkyne and steric bulk on the terminal carbon to achieving high *ee*. Indeed, our initial attempts to expand the scope of asymmetric, Ag-catalyzed NT to encompass asymmetric amidations of benzylic, allylic, and unactivated methylene C–H bonds were not promising; the limited modularity of the initial synthesis of (S,S)-Min-BOX hampered efforts to identify key interactions be-tween substrate and catalyst that could be tuned to improve scope. In light of these challenges, we aspired to develop a modular approach to the Min-BOX scaffold and to gain a more complete picture of catalyst features responsible for high chemo-, site-, and enantioselectivity with diverse types of C–H bonds. In this work, we report the design and synthesis of several new BOX ligands, along with combined experimental and computational studies, that provide key insights to inform cata-lyst designs that display broad scope for accessing enantioen-riched building blocks for the synthesis of 1,3-aminoalcohols.

RESULTS

Benchmarking (S,S)-Min-BOX for asymmetric amidations of diverse C–H bonds

Studies to explore site- and enantioselective NT with (S,S)-Min-BOX were initiated using three simple carbamates **1a–c**, bearing a benzylic, allylic, and unactivated C–H bond, respectively (Table 1).[20] Treatment of **1a** with PhIO, 5 mol % AgClO$_4$, and 2.5 mol % (S,S)-Min-BOX at −10°C for 48 h resulted in a moder-ate 60% yield of **2a** in a promising 90% *ee* (Table 1, entry 1). The site selectivity was excellent and no five-membered ring product was observed. This stands in contrast to all other reported cata-lysts for NT of carbamates, which give either the five-membered

heterocycles (Scheme 1A) or mixture of five- and six-membered rings. The excess AgClO$_4$ serves as a Lewis acid to break down the polymeric PhIO and increase the overall reaction rate and conversion. Control experiments show minimal background re-action promoted by unligated AgClO$_4$. Reducing the tempera-ture in the reaction of **1a** to **2a** to −20°C (entry 2) required increased catalyst loading and time; both the conversion and yield were improved, although the *ee* was similar, suggesting no benefit to temperatures lower than −10°C. Carrying out the reaction at room temperature (RT) reduced the *ee* to 82% (entry 3) but gave complete conversion to **2a** in 99% yield. In cases where the product *ee* is easily increased via simple recrystalliza-tion, this minimal reduction in *ee* may be readily compensated for by the higher conversions and yields observed at RT. Ultimately, increasing the catalyst loading to 10 mol % AgClO$_4$ and 5 mol % (S,S)-Min-BOX and running the reaction at −10°C gave a good balance between conversion and *ee* (entry 4); these conditions were adopted for studies of the substrate scope.

Substrate **1b**, bearing an unhindered allylic C–H bond, showed a significant decrease in *ee* to 54% using (S,S)-Min-BOX (entry 5). Both chemo- and site-selectivity were excellent, with no competing formation of the aziridine or the five-membered ring. Substrate **1c**, which contains an unactivated C(sp^3)–H bond (entry 6), showed both poor conversion and low *ee* using (S,S)-Min-BOX as the ligand. In addition, small amounts of the five-membered ring were formed. These preliminary results highlight the need for better catalyst designs for asymmetric Ag-catalyzed NT.

Scope of asymmetric benzylic C–H bond amidation

Although the (S,S)-Min-BOX ligand did not show promise as a general catalyst for asymmetric NT, we wanted to explore the potential for asymmetric amidations of benzylic C–H bonds. We reasoned these studies would provide insight into potential catalyst/substrate interactions that could be tuned to impact the enantiomeric excess (*ee*) in a predictable way. This informa-tion could inform computational studies to develop a feasible stereochemical model and deliver higher *ee* in the amidations of diverse C–H bonds, including challenging allylic and unacti-vated C–H bonds.

With optimized conditions in hand, the scope of the enantiose-lective C–H amidation was explored (Scheme 2) and the perfor-mance of (S,S)-Min-BOX(AgClO$_4$) assessed compared to Rh and Ru catalysts (Scheme 1A). In general, the high *ee* of the reaction was maintained across diverse carbamates containing benzylic C–H bonds. The six-membered ring products were obtained, despite using more easily accessible carbamates as compared to sulfamates. Changing the electronics of the arene though the addition of electron-withdrawing or electron-donating groups in the *p*-position (**2a**, **3a–7a**) did not significantly impact *ee*. Precursor **6**, bearing a *p*-OMe group, gave **4a** in 90% *ee*, while **7**, bearing a *p*-CF$_3$ group, gave **7a** in a similar *ee* of 88%. Interestingly, this result contrasts with those observed with both the Du Bois Rh$_2$(S-NAP)$_4$ and the Blakey Ru(pyBOX) cata-lysts,[13,14] although steric effects cannot be completely ruled out in these examples. As expected, more electron-poor C–H bonds typically underwent amidation at slower rates under stan-dard conditions, resulting in only ~50% conversion for **4a–6a**.
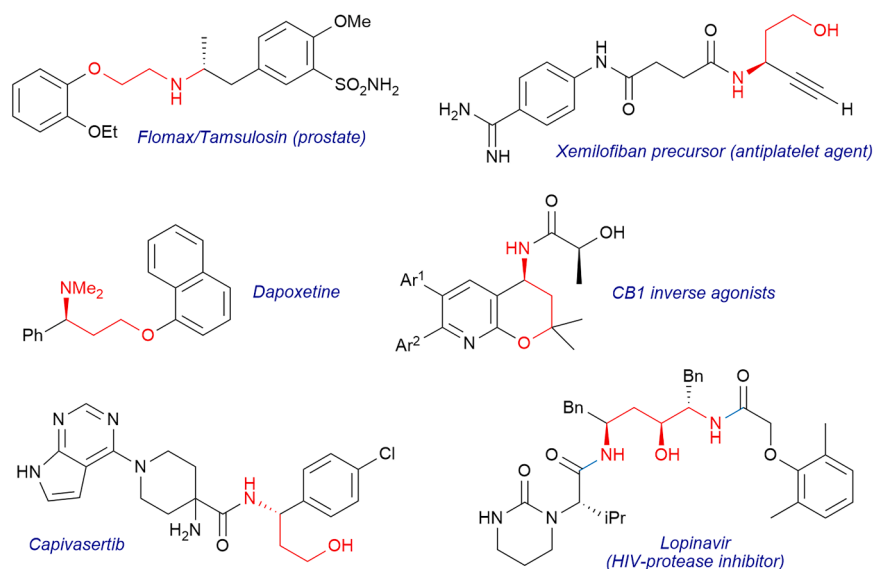
Figure 1. Aminoalcohol-containing bioactive molecules

However, increasing the amount of the Ag salt to 20 mol % improved conversion with little impact on the *ee*. Substitution at the α-position of the carbamate tether in **8** enhanced the reactivity to furnish **8a** in excellent yield and *ee*, even at reduced catalyst loadings.

Interestingly, the addition of a Me group at the *m*-position of **9** maintained a high 90% *ee* in **9a**, while moving the Me group to the *o*-position in **10** lowered the *ee* slightly to 80% in **10a**. Electron-rich heterocycles were also tested; furan **11a** was obtained in good *ee*, with the lower yield attributed to competing oxidative degradation of the furan ring. While indole derivative **12** was poorly reactive at −10°C, a moderate yield and *ee* of **12a** could be obtained at RT.

Substrates containing a stereogenic carbon were also investigated to probe how the nature of the catalyst impacts the diastereoselectivity of the Ag-catalyzed amidation. Carbamates **13** and **14** were prepared in enantioenriched form from the corresponding secondary alcohols and individually subjected to the reaction conditions. Utilizing (*S,S*)-Min-BOX with the (*R*)-enantiomer **14** increased the *dr* for the *syn* diastereomer **14a** to >20:1, compared to the 3.4:1 *syn:anti* ratio observed when the same reaction was run with an achiral BOX ligand. Subjecting the (*S*)-enantiomer **13** to standard reaction conditions resulted in the catalyst selecting for the typically disfavored *anti*-diastereomer **13a** in a 5.7:1 *dr*. This is particularly noteworthy, as enantioenriched *trans*-1,3-aminoalcohols are not accessible using other reported catalyst systems, which overwhelmingly favor the *syn* diastereomer.[3–6] When **13** was treated with (*R,R*)-Min-BOX, representing the matched case, the *syn* diastereomer was favored to yield the enantiomer of **14a**. In the same vein, treatment of **14** with (*R,R*)-Min-BOX gave the enantiomer of **13a** favoring the *anti*-diastereomer over the *syn* with a 6.5:1 *dr*. In this manner, we could obtain access to all four diastereomers of the 1,3-aminoalcohol products from reaction of **13** and **14** using either enantiomer of the Min-BOX ligand.

To further challenge our asymmetric amidation chemistry, a carbamate **15** bearing a tertiary benzylic C–H bond was investi-gated. With a typical racemic catalyst, NT likely occurs either through a concerted C–H amidation or by H-atom abstraction, followed by a rapid radical rebound. However, we were curious whether a mismatch between (*S,S*)-Min-BOX and the stereochemistry at a racemic tertiary C–H bond could lead to a longer-lived radical intermediate, where the initial stereochemistry could be ablated and reset by the catalyst. Amidation of **15** under standard conditions gave a 49% yield of product **15a** and 49% recovery of **15**, with 48% *ee* observed for both compounds. This suggests a scenario involving moderate kinetic resolution by the Ag/(*S,S*)-Min-BOX catalyst, influenced by the small difference between the two activation barriers for C–H amidation of (*R*)-**15** vs. (*S*)-**15**. We were pleased to observe that (*S,S*)-Min-BOX(AgClO₄) effectively desymmetrized the benzylic C–H bonds in good *ee*. Subjecting achiral carbamates **17** and **18** to standard conditions resulted in effective desymmetrization of both compounds to provide the corresponding benzylic amines **17a** and **18a** in excellent yield, *dr*, and *ee*. When **18** was treated with (*R,R*)-Min-BOX(AgClO₄), the enantiomer of **18a** was obtained.

Finally, we were curious if the (*S,S*)-Min-BOX ligand could furnish good *ee* in Ag-catalyzed amidations of homobenzylic carbamates to deliver enantioenriched 1,2-aminoalcohols. Reaction of **16** at RT gave a good yield of **16a**, albeit in a low 34% *ee*; *ee* was not improved by lowering the temperature, highlighting the need for further catalyst optimization efforts. Nonetheless, this result, when combined with results showing the impact of the sterics of arene substitution on the *ee* (Scheme 2, **9a**–**10a**), provided valuable information to inspire our computational investigations on factors affecting catalyst-substrate interactions and the effectiveness of enantioinduction in the selectivity-determining transition states (Figures 2, 3, 4, and 5, *vide infra*).

Computational explorations of asymmetric Ag-catalyzed benzylic C–H bond amidation with (*S,S*)-Min-BOX

Density functional theory (DFT) calculations[23] were performed to investigate the origin of the *ee* in the Ag-catalyzed benzylic C–H amidation and to better understand why the (*S,S*)-Min-BOX ligand leads to high *ee* with benzylic and heterobenzylic precursors but is less effective with substrates containing allylic (Table 1, **1b**) or unactivated methylene C–H bonds (**1c**). DFT and local coupled cluster theory [PNO-LCCSD(T)-F12][24,25] calculations indicated that the singlet Ag nitrene C–H insertion pathway is more favorable than the competing triplet pathway (see Figure S1 for details).[26–29] This singlet pathway involves concerted C–H bond cleavage and C–N bond formation without
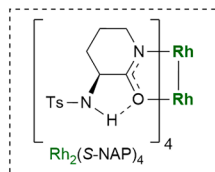
A Previous asymmetric amidations to furnish 1,3- and 1,2-aminoalcohols
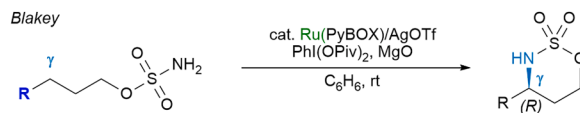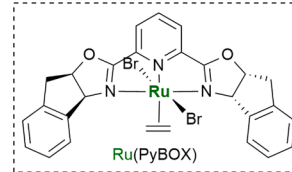
sulfamate nitrene precursors

Du Bois
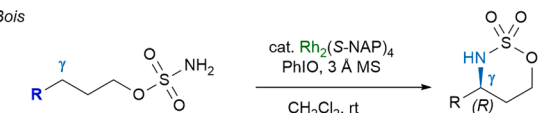
R	
Ph	85%, 92% ee
p-OMePh	89%, 83% ee
p-CF3Ph	50%, 56% ee
(E)-MeCH=CH	51%, 54% ee
(Z)-MeCH=CH	70%, 82% ee

Rh₂(S-NAP)₄

Blakey

R	
Ph	84%, 84% ee
p-OMePh	68%, 90% ee
p-CF3Ph	56%, 80% ee
(E)-MeCH=CH	60%, 89% ee
(Z)-MeCH=CH	42%, 50% ee

Ru(PyBOX)

carbamate nitrene precursors

Davies

72%, 82% ee

Rh₂(S-TCPTAD)₄
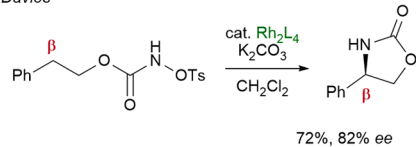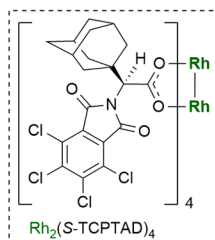
Meggers
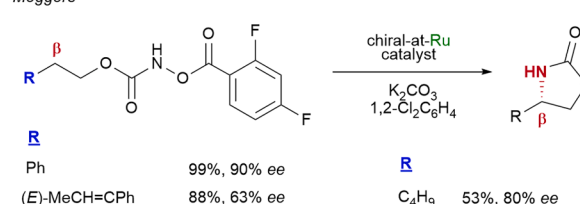
R	
Ph	99%, 90% ee
(E)-MeCH=CPh	88%, 63% ee

R	
C4H9	53%, 80% ee

B **This work:** General catalysts for silver-catalyzed asymmetric C-H amidation

plus **10** other MinBOX analogs

(S,S)-MinBOX
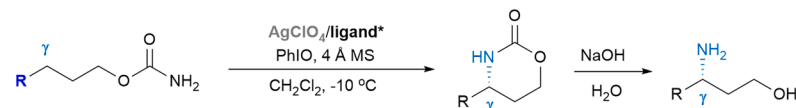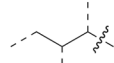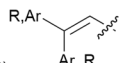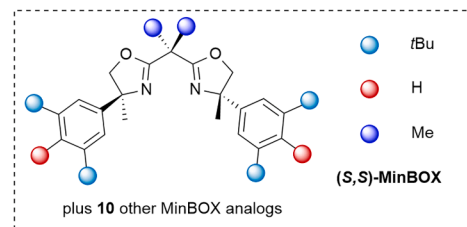
- silver as an inexpensive metal
- modular, tunable ligand platform
- low sensitivity to substrate electronics
- computational insights for new ligands
- expanded substrate scope

ee >90%   ee <30%

Scheme 1. Prior and new asymmetric C–H amidations via NT to furnish amino alcohols
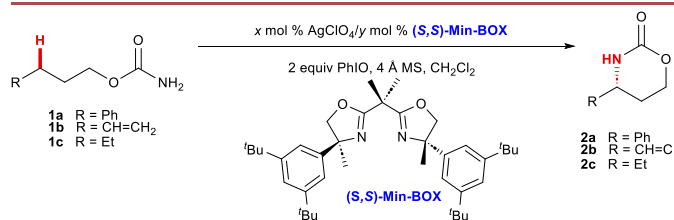(A) Previous asymmetric amidations to furnish 1,3- and 1,2-aminoalcohols.
(B) This work: general catalysts for Ag-catalyzed asymmetric C–H amidation.

the formation of a discrete alkyl radical intermediate; therefore, the ee is determined in this concerted C–H insertion transition state (TS). The most stable C–H insertion TS isomers with the benzylic substrate **1a** (Figure 2) involve a four-coordinate square-planar Ag-nitrene complex, where the carbamate carbonyl coordinates to the Lewis acidic Ag center. Several alternative TS isomers were also considered, including a trigonal planar Ag nitrene lacking the carbamate carbonyl–Ag coordination, a TS with a partially dissociated monodentate Min-BOX ligand having only one oxazoline nitrogen bound to the Ag, and, finally, a TS having an N,O-bidentate-binding mode for (S, S)-Min-BOX (see Figures S2 and S3 for details). All of these alternative TS isomers are higher in energy than those involving the four-coordinate square-planar Ag-nitrene complex where the carbamate carbonyl group is coordinated to Ag. This C–H insertion mechanism involving a singlet square-planar Ag nitrene is consistent with our recent computational study of NT using an achiral 2,2′-isopropylidenebis(4,4′-dimethyl-2-oxazoline)-supported (dmBOX) Ag catalyst.

Next, we analyzed the origins of ee in the benzylic C–H amidation of **1a**. Two ring-flipped conformers of the seven-membered cyclic C–H insertion TS were located for the activation of each prochiral benzylic C–H bond (Figure 2). The computed ee is consistent with the experimental results, where the most favorable C–H insertion transition state **TS1** ($\Delta G^{\ddagger}$ = 6.6 kcal/mol with respect to the Ag-nitrene intermediate) leads to the observed major enantiomeric product, (R)-**2a**. The two transition state conformers (**TS2** and **TS4**) that lead to the S enantiomer of the product (S)-**2a** are both 3.9 kcal/mol higher in energy than **TS1**. The ee is attributed to steric repulsions between the Ph substituent on the benzylic substrate and the C2-symmetric (S, S)-Min-BOX ligand that led to greater distortion of the disfavored transition states. In all four C–H insertion transition states (**TS1**–**TS4**), the nitrene moiety in the four-coordinate Ag complex is

Table 1. Initial screening of Ag-catalyzed amidations supported by (S,S)-Min-BOX

Entry	Substrate	Mol % Ag	Mol % lig	T (°C)	Time (h)	Yield 2 (ee)
1	1	5	2.5	−10	48	60% **2a** (90%)
2	1	20	10	−20	72	75%[a] **2a** (92%)
3	1	20	10	rt	12	99%[a] **2a** (82%)
4	1	10	5	−10	48	90%[a] **2a** (90%)
5	2	10	5	−10	48	79%[a] **2b** (54%)[b]
6	3	10	5	−10	24	26%[a] **2c** (38%)[b,c]

Yields determined by ^{1}H NMR with mesitylene and Me₃PhSiH as internal standards.
[a]Isolated yields.
[b]ee was determined after benzylation.
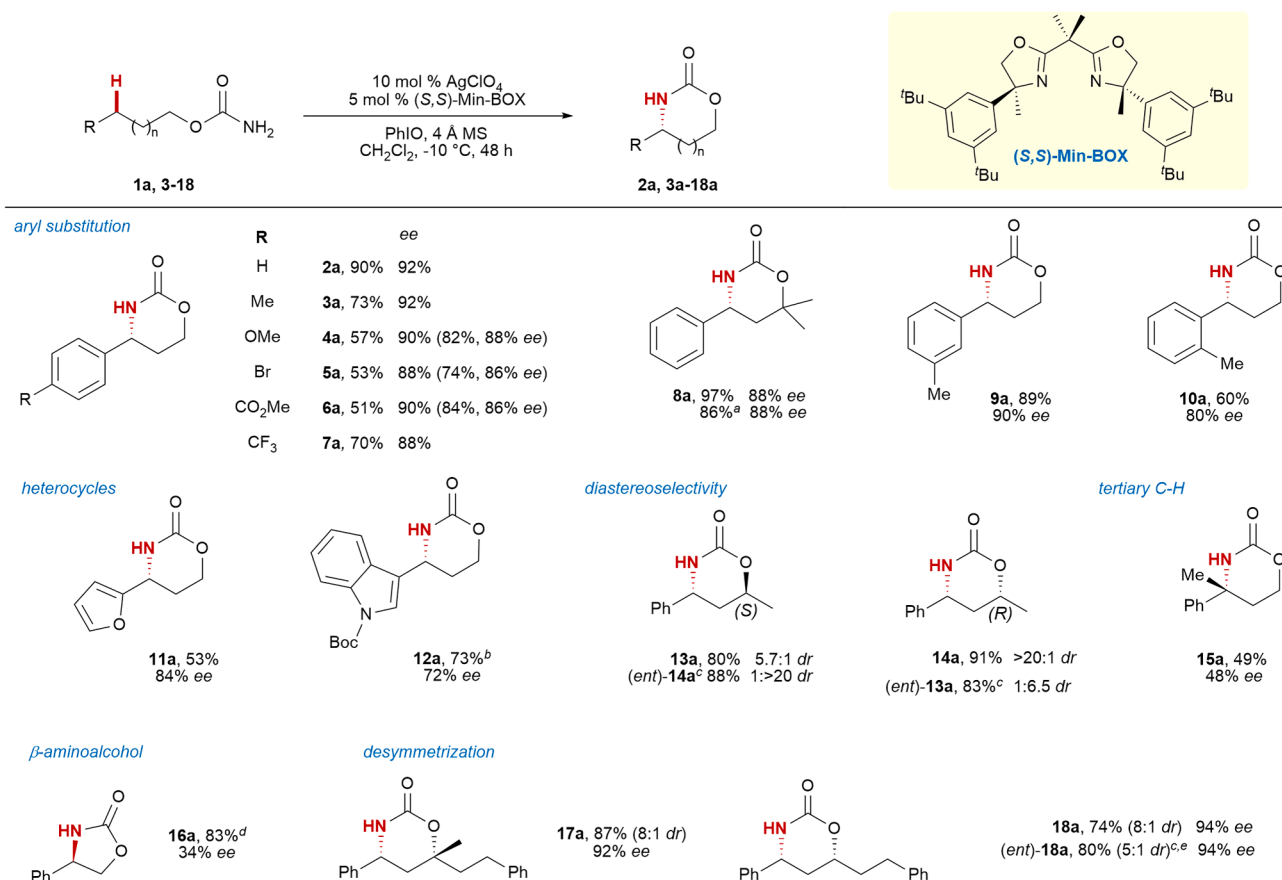[c]5% of the five-membered ring.

slightly distorted from the preferred square-planar geometry due to steric repulsions with the Ar group on the (S,S)-Min-BOX ligand located in quadrant **IV**. This sterically induced distortion is more profound in **TS2** and **TS4**, where the Ph group of the substrate would be placed in a quadrant (**IV**) occupied by the bulky Ar group if the nitrene was not distorted. In the optimized structures of **TS2** and **TS4**, the Ph group is placed in the less occupied quadrant **I**, resulting in a more distorted square-planar geometry. Such distortion weakens the Ag–carbamate carbonyl coordination and leads to longer Ag···O(carbonyl) distances in **TS2** and **TS4** (2.22 and 2.20 Å, respectively) than those in **TS1** and **TS3** (both are 2.18 Å). In **TS1** and **TS3**, the Ph group is placed in the unoccupied quadrant **I**, and thus such ligand-substrate steric repulsions are diminished. In addition, **TS1** is stabilized by a C–H/π interaction between the Ph group on the substrate and the t-Bu group on the ligand. The ring-flipped TS conformer **TS3** is 2.2 kcal/mol less stable than **TS1** because the Ph group is in a pseudoaxial position, rather than the pseudoequatorial position as in **TS1**.

Next, we investigated substrate effects on ee by comparing the C–H insertion TS using a benzylic substrate with a shorter tether (**16** in Scheme 2; Figure 3). The computed enantioselectivities for **16** are predicted to be lower than those of **1a** ($\Delta\Delta G^{\ddagger}$ = 2.5 kcal/mol for **16**, compared to $\Delta\Delta G^{\ddagger}$ of 3.9 kcal/mol for **1a**), which is consistent with the lower experimentally observed er. In the C–H insertion reaction with **16**, the ligand-substrate steric repulsion in **TS6** leading to the minor product (S)-**16a** is also diminished, because the six-membered cyclic TS is sterically less encumbered than the seven-membered TS with **1a** as the precursor. The greater ligand-substrate distance allows the Ph group on the substrate to be placed in the occupied quadrant (**IV**) without distorting the Ag nitrene and the preferred square-planar geometry can still be maintained. **TS5** leading to the major enantiomeric product contains a ligand-substrate C–H/π interaction similar to **TS1**; however, due to the smaller ring size, a

greater substrate distortion is required to orient the Ph group toward the Ar group in interactions between the t-Bu group on the Min-BOX ligand and the Ph group on the benzylic substrate in the TS leading to the major enantiomeric product. The lower er observed with substrates with a shorter tether (e.g., **16**) is because one or both of these interactions are diminished. Taken together, the computed C–H insertion transition states with substrates **1a** and **16** revealed two concurrent factors affecting ee: ligand-substrate steric repulsions that destabilize the TS leading to the minor enantiomeric product, and C–H/π with respect to the singlet Ag-nitrene intermediate. Thus, lessons learned from these key computations that may help inform better ligand designs include (1) the lowest-energy conformer that leads to the major enantiomer must be capable of maintaining a square-planar geometry at the Ag center; (2) attractive interactions between the substrate and ligand in the lowest-energy conformer leading to the major enantiomer are beneficial; (3) the ability to distort the Ag from a square-planar geometry through repulsive or steric interactions in the conformers that lead to the minor enantiomer are helpful in improving ee; and (4) the lack of any stabilizing non-covalent interactions (NCIs) in conformers leading to the minor enantiomer, as compared to the conformers leading to the major enantiomer, have the potential to aid in improving the ee of the reaction.

Computational explorations of asymmetric Ag-catalyzed allylic C–H bond amidation with (S,S)-min-BOX

Given the low ee observed in the NT of **1b** (Table 1, entry 5, vide supra), we undertook computational studies to better understand the discrepancy in the performance of (S,S)-Min-BOX for asymmetric amidation of benzylic vs. allylic C–H bonds. The computed ee for **1b** was found to be lower than that of **1a** ($\Delta\Delta G^{\ddagger}$ = 0.7 kcal/mol compared to $\Delta\Delta G^{\ddagger}$ of 3.9 kcal/mol for **1a**), which is consistent with the lower observed experimental ee (Figure 4). In the allylic C–H insertion transition state (**TS8**)

R		ee
H	**2a**, 90%	92%
Me	**3a**, 73%	92%
OMe	**4a**, 57%	90% (82%, 88% ee)
Br	**5a**, 53%	88% (74%, 86% ee)
CO₂Me	**6a**, 51%	90% (84%, 86% ee)
CF₃	**7a**, 70%	88%

aryl substitution

8a, 97% 88% ee
86%ᵃ 88% ee

9a, 89%
90% ee

10a, 60%
80% ee

heterocycles

11a, 53%
84% ee

12a, 73%ᵇ
72% ee

diastereoselectivity

13a, 80%   5.7:1 dr
(ent)-**14a**ᶜ 88% 1:>20 dr

14a, 91% >20:1 dr
(ent)-**13a**, 83%ᶜ 1:6.5 dr

tertiary C-H

15a, 49%
48% ee

β-aminoalcohol

16a, 83%ᵈ
34% ee

desymmetrization

17a, 87% (8:1 dr)
92% ee

18a, 74% (8:1 dr) 94% ee
(ent)-**18a**, 80% (5:1 dr)ᶜ,ᵉ 94% ee

Yields and *ee* values in parenthesis were run with 20 mol % AgClO₄. ᵃ 5 mol % AgClO₄, 2.5 mol % (*S,S*)-Min-BOX. ᵇ 20 mol % AgClO₄, 10 mol % (*S,S*)-Min-BOX, room temperature (rt). ᶜ Results were repeated with (*R,R*)-Min-BOX. ᵈ 18-20 h at room temperature. ᵉ The enantiomer of **18a** was obtained.

Scheme 2. Scope for asymmetric Ag-catalyzed amidation of benzylic C–H bonds

leading to the minor product (*S*)-**2b**, the smaller alkenyl group in **1b** compared to the Ph group in **1a** diminishes the steric repulsion with the (*S,S*)-Min-BOX ligand. This means that the alkenyl group can be placed in the occupied quadrant **IV** without distorting the square-planar geometry of the Ag nitrene. Moreover, in **TS5** leading to the major product (*R*)-**2b**, the stabilizing NCIs between the ligand and the smaller alkenyl group are weaker than the C–H/π interaction observed in **TS1** with the benzylic substrate **1a**. Therefore, both factors lead to diminished *ee* with the allylic substrate. As was seen for **16**, two concurrent factors affecting the *er* using **1b**: ligand-substrate steric repulsions that destabilize the TS leading to the minor enantiomeric product, and C–H/π with respect to the singlet Ag-nitrene intermediate. The (*S,S*)-Min-BOX ligand was used in the calculations.

We surmised that the *ee* of challenging substrates, such as **1b**, might be enhanced by rationally tuning either the substituents on the Min-BOX ligand scaffold or the steric properties of the substrate to further enhance the stabilizing NCIs in the favored TS, as well as the steric repulsions and substrate distortions in the disfavored TS. Because the computed TS structures indicated insufficient catalyst-substrate interactions due to the smaller size of the allyl moiety in **1b** (Figure 4), we postulated that the desired interac-

tions could be enhanced by using a more hindered (*S,S*)-Wen-BOX ligand, where the 3,5-di-*tert*-Bu phenyl substituents in (*S,S*)-Min-BOX were replaced with 3,5-di-Ar phenyl groups. The computations did indeed predict a small increase of *ee* in the C–H amidation of **1b** (Figure 5, top, $\Delta\Delta G^{\ddagger}$ = 1.3 kcal/mol compared to 0.7 kcal/mol in the reaction with (*S,S*)-Min-BOX). In this case, the transition state (**TS9**) leading to the major product may be stabilized by C–H/π interactions between the alkenyl C–H bond on the substrate and the newly introduced Ph group on the ligand. In addition, the transition state leading to the minor product, **TS10**, suffers from greater ligand-substrate steric repulsions in the occupied quadrant **IV** that distort the Ag nitrene to the non-square-planar conformation with a longer Ag···O(carbonyl) distance (2.19 Å, vs. 2.15 Å in **TS9**). Although the *er* improvement is predicted to be small, in part due to the relatively small energy penalty for substrate distortion to avoid unfavorable steric repulsions in the disfavored C–H insertion TS, we were excited to test this computational prediction through the exploration of other new ligands for asymmetric allylic C–H amidation (see Scheme 3, *vide infra*).

As computational models (Figures 2, 3, and 4) indicated that substrate identity is also expected to exert a large effect on the
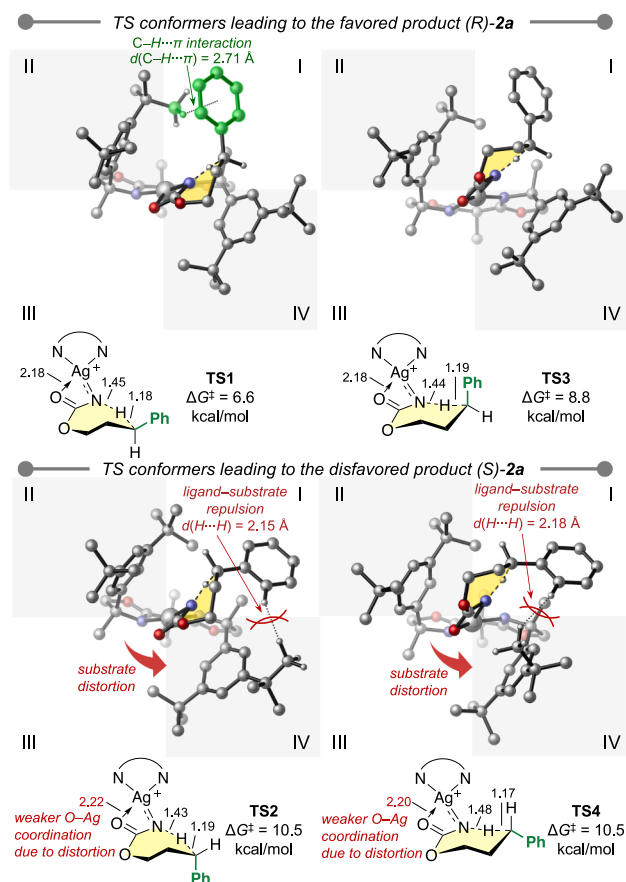
Figure 2. C−H insertion TS structures of the asymmetric NT of benzylic substrate 1a

Gibbs free energies of activation are with respect to the Ag-nitrene intermediate. The (S,S)-Min-BOX ligand was used in the calculations.

distortion or stabilization of the relevant flexible seven-membered ring transition states, we wanted to assess how the use of more sterically demanding alkenes might either enhance or hinder productive catalyst-substrate interactions. Thus, the computed transition states of the styrenyl precursor **19** (Figure 5) using the (S,S)-Min-BOX ligand were compared to the allylic substrate **1b** with the same ligand, with the $\Delta\Delta G^{\ddagger}$ values calculated to be 2.2 and 0.7 kcal/mol for **19** and **1b**, respectively (Figure 5, bottom). The newly introduced Ph group on **19** enables stabilizing C–H/π interactions with the *tert*-Bu group on the (S,S)-Min-BOX ligand (quadrant **II**) in the **TS11** that would lead to the major experimentally observed enantiomeric product. In addition, replacing the vinyl group of **1b** with the larger styrenyl moiety increases ligand-substrate steric repulsion in the **TS12** that leads to the minor enantiomeric product, producing similar substrate distortions that we observed in computations of other disfavored TS isomers, including **TS2** and **TS10**. Therefore, if the higher predicted *er* with **19** could be verified experimentally, this might indicate that the alkenyl substituent on the substrate also affects non-covalent ligand-substrate interactions and substrate distortion and, ultimately,

the *ee* of the amidation product. These results prompted us to experimentally explore a much broader scope of alkenes bearing various substitution patterns to further understand these ligand/substrate effects on both the reactivity and *ee* of the asymmetric amidations of diverse allylic C–H bonds (see Scheme 4, *vide infra*).

Modular route to new BOX ligands for asymmetric NT informed by computational investigations

With computational studies in hand to shed insight into how changes to the features of the (S,S)-Min-BOX ligand and/or the substrate might impact *ee*, we required a more modular route to the Min-BOX scaffold to broaden the scope of asymmetric amidation to include challenging allylic and unactivated C(sp³)–H bonds. Our first-generation synthesis suffered from several drawbacks,[20] including an initial asymmetric Rh-catalyzed hydroformylation that requires bis[(S,S,S)-DiazaPhos-SPE], a complex and commercially unavailable ligand.[21] Access to the enantiomer of DiazaPhos-SPE was not available; thus, only (S, S)-Min-BOX could be prepared using our original route. Finally, the use of hydroformylation as a key step limits the modularity of the synthesis to the installation of a Me group at the fully substituted sp³ carbon of the BOX.

To address these issues and provide a reliable and versatile approach to analogs of both (S,S)-Min-BOX and (R,R)-Min-BOX, a new route to this class of ligands was developed (Scheme 3A). This strategy enables easy manipulation of three diverse sites in the ligand, including the alkyl group at the chiral quaternary carbon, the substitution pattern on the aryl ring, and the nature of the ligand backbone, which can be manipulated to change the bite angle of the catalyst. Asymmetric Rh-catalyzed boronic ester addition to imine **a** gave **b**,[22] which was further elaborated to (S,S)-Min-BOX using standard procedures. Employing the enantiomer of *tert*-butylsulfinamide ligand gave facile access to (R,R)-Min-BOX, which was unavailable through our previous route.[20] In addition, the modular nature of the approach to this class of ligands enables the backbone to be altered, as highlighted in blue in the transformation of **c** to (S, S)-Min-BOX (**A**), (S,S)-H,H-Min-BOX (**I**), and (S,S)-Cyp-Min-BOX (**J**) (Scheme 3A). The (S,S)-H,H-Min-BOX was both a ligand of interest as well as an intermediate for further versatile modifications to the backbone. Thus, this strategy represents a highly modular approach toward altering the bite angle of Min-BOX-type ligands to determine the impact on *ee*.

Based on guidance from our computational studies, 10 additional ligands **B–K** were synthesized (Scheme 3B). The (S,S)-Wen-BOX ligand (**B**) was targeted based on computational insights from Figure 5, where replacing the *tert*-butyl groups of (S,S)-Min-BOX with aryl groups is predicted to lead to a larger ΔΔG‡ between the TS leading to the major and minor enantiomers in the asymmetric amidation of the allylic C–H bond of **1b**. Inspired by computational results, the idea behind the design of (R,R)-Em-BOX (**D**) is to restrict rotation around the Ar−C(sp³) bond of the 3,5-di-*tert*-butyl groups to provide additional rigidity to the catalyst and thereby increase the steric repulsions found in the unfavorable TS. Computations also suggested that increasing the electron-donor ability of the aryl group may improve selectivity-determining C−H/π interactions (see

lowest-energy TS conformers with benzylic substrate **16**
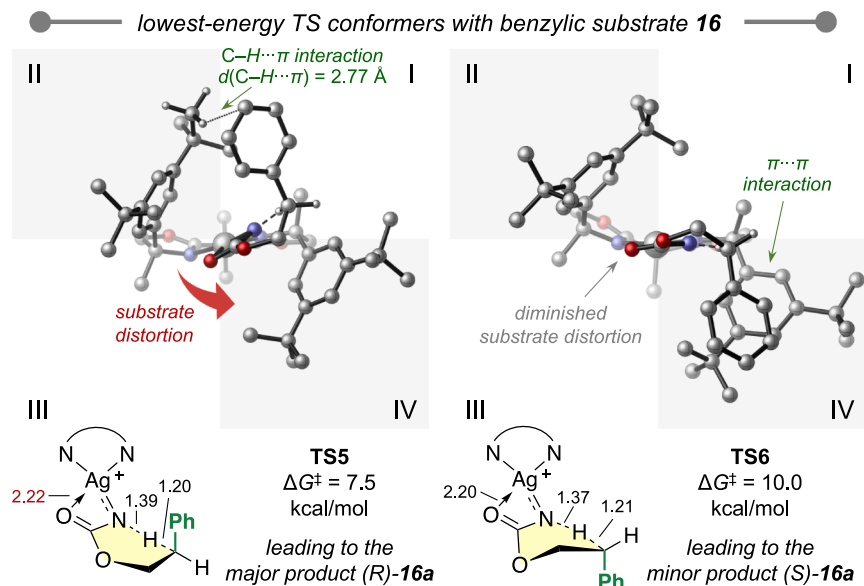
Figure 3. Origins of diminished *ee* in the C–H amidation of benzylic substrate 16 with a shorter tether

Gibbs free energies of activation are in kcal/mol. This distortion leads to a longer Ag···O(carbonyl) distance of 2.22 Å in **TS5**, compared to 2.20 Å in **TS6**. (*S,S*)-Min-BOX ligand was used in the calculations.

are important for high *ee*, the extended conjugation of (*S,S*)-Wen-Box **B** increased *ee* for **20a** to 72%. The additional rigidity of (*R,R*)-Em-BOX **D** improved both the yield and *ee* to 82% and 75%, respectively. Finally, both (*S,S*)-H,H-Min-BOX **I** and (*S,S*)-Cyp-Min-BOX **J** also improved the *ee*, suggesting that altering the bite angle of the ligand may be beneficial when small groups are present on the terminal carbon of the alkene, although this effect requires further investigation.
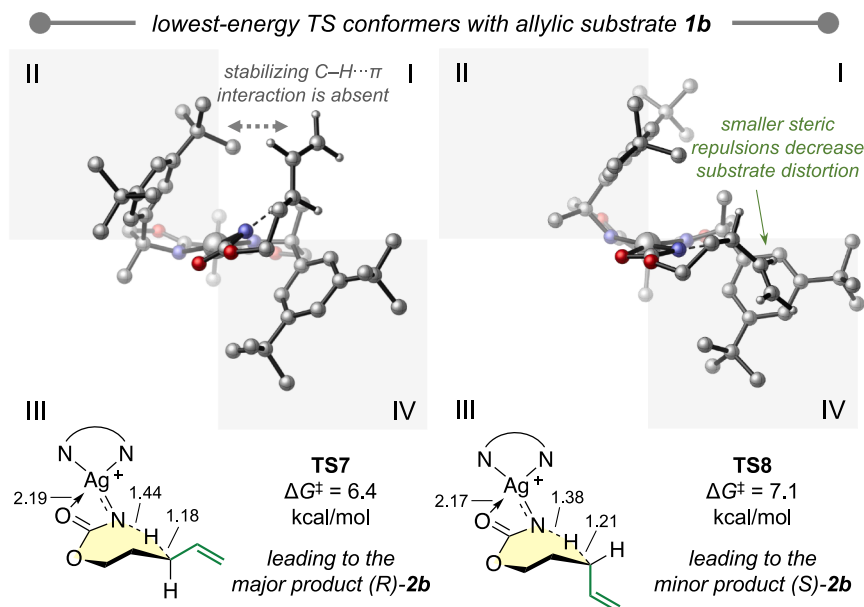
The impact of ligand identity on the *ee* of products resulting from amidation of **1c**, **21**, and **22** (Scheme 3C), which bear unactivated alkyl C(sp³)–H bonds, was complicated by issues of site-selectivity to give mixtures of six- and five-membered heterocyclic products. While control over both site- and enantioselectivity are ultimately of interest, we focused on the *ee* of the six-membered ring products **2c**, **21a**, and **22a**. The importance of having a π-bearing substituent adjacent to the C–H bond undergoing amidation was highlighted by comparing results obtained with **20** to those with **1c**, which lacks an alkene. A maximum *ee* of 40% of **2c** at RT was obtained with (*S,S*)-Wen-BOX **B** and (*R,R*)-H-Ph-QT-BOX **F** ligands, significantly lower than the 77% *ee* noted for **20a**. These results are supported by our computational models, which suggest key NCIs between the alkene and catalyst contribute to higher *ee*, interactions that are lacking in the reaction of **1c**.

The impact of the sterics of the adjacent alkyl group on site- and enantioselectivity was assessed with **21** and **22**, bearing cyclohexyl and *tert*-butyl groups adjacent to the target C–H bond. With **21**, (*S,S*)-Min-BOX **A** gave only 43% *ee*, while (*S,S*)-Wen-BOX **B** significantly improved both the yield and *ee* of **21a** to 61% and 67%, respectively. The (*R,R*)-H-Ph-QT-BOX **F** and the (*R,R*)-*p*-CF₃-Ph-QT-BOX ligand **G** gave similar results to (*S,S*)-Wen-BOX **B**; all other ligands either gave lower ratios of **21a:21b** or a lower *ee*. We hypothesize C–H/π interactions between a cyclohexyl C–H bond and the aromatic groups of ligands **B**, **F**, and **G** increase *ee*; the electronic effects support this, as **E** gave a reduced *ee* of 28%. Steric repulsions between the cyclohexyl and bulky *tert*-butyl and groups on ineffective ligands result in low *ee*. Interestingly, the *tert*-butyl-substituted precursor **22** showed different trends compared to **21**. In this case, (*S,S*)-Min-BOX **A**, (*R,R*)-Em-BOX **D**, and (*S,S*)-Cyp-Min-BOX **J** gave comparable results, with all other ligands giving either poor ratios of **22a:22b** or lower *ee*. These results point to the potential importance of the directionality of the C–H bond in the

Figure 3, *vide supra*). Thus, ligands (*S,S*)-*m*-(OMe)₂-Ph-QT-BOX (**C**), (*R,R*)-*p*-OMe-Ph-QT-BOX (**E**), (*R,R*)-*p*-CF₃-Ph-QT-BOX (**G**), and (*R,R*)-H-Ph-QT-BOX (**F**) were prepared to assess the impact of aryl electronics on the *er* independent of the sterics; these are easier to access than their 3,4,5-trisubstituted counterparts. The impact of extended conjugation in the aromatic ring attached to the quaternary stereogenic center of the ligand was assessed through the synthesis of (*R,R*)-2-naphthyl-QT-BOX (**H**). Full details of the syntheses of all of the ligands highlighted in Scheme 3B can be found in Scheme S1.

Ligands **A–K** from Scheme 3B were first benchmarked with four different challenging substrates consisting of a *trans*-Me-substituted alkene **20**, a linear alkyl-substituted precursor **1c**, plus two substrates containing unactivated alkyl C(sp³)–H bonds adjacent to a cyclohexyl (**21**) and a *tert*-butyl group (**22**). Chemocatalyzed asymmetric amidations of unactivated prochiral C–H bonds to form enantioenriched 1,3-aminoalcohols in particular remain difficult for metal-catalyzed NT. This is especially true when the substrate lacks either a π bond or heteroatom on the alkyl chain that can engage in strong attractive directing NCIs to drive *ee* in a predictable way. In these cases, repulsive steric interactions play a larger role in impacting *ee*, yet the conformational flexibility and steric differences engendered by branching means that one catalyst may not be suitable to furnish high *ee* for all types of unactivated C–H bonds. Our unique BOX ligand library is ideally suited to explore how features of the alkyl substituent impact the asymmetric NT (Scheme 3C; additional optimization studies are included as Table S1).

Reactions were initially carried out at RT to speed throughput and maximize conversion, with the idea of optimizing promising ligands at lower temperatures. Valuable trends were noted (Scheme 3C); for example, asymmetric amidation of the allylic C–H bond of **20** to **20a** gave 64% *ee* with the parent (*S,S*)-Min-BOX **A**, but, in support of our hypothesis that attractive NCIs

lowest-energy TS conformers with allylic substrate **1b**

stabilizing C–H···π interaction is absent

smaller steric repulsions decrease substrate distortion

TS7
ΔG‡ = 6.4 kcal/mol
leading to the major product (R)-2b

TS8
ΔG‡ = 7.1 kcal/mol
leading to the minor product (S)-2b

Figure 4. Origins of diminished *ee* in the C–H amidation of allylic substrate 1b
Gibbs free energies of activation are in kcal/mol.

substrate on *ee*. Essentially, groups lacking a π bond located adjacent to the reactive C–H negate the ability of attractive NCIs in the TS to impact *ee*, forcing a reliance on repulsive steric interactions to control *ee*. This was further tested with (*R,R*)-JAM-BOX **K**, which was synthesized from the same amino alcohol used to prepare **J**. This ligand combines elements of both ligands **D** and **J** to amplify C(sp³)–H-π interactions and resulted in significant improvements to the *ee* of both **2c** and **21a**, with the latter increasing to 81% *ee*.

Optimizing new BOX ligands for asymmetric NT of benzylic and allylic C–H bonds

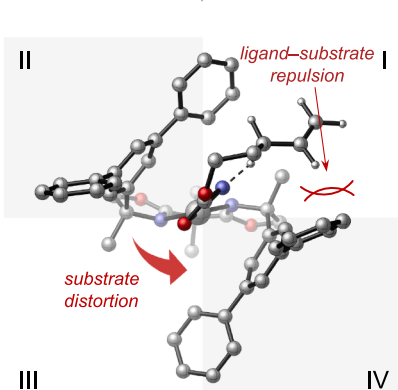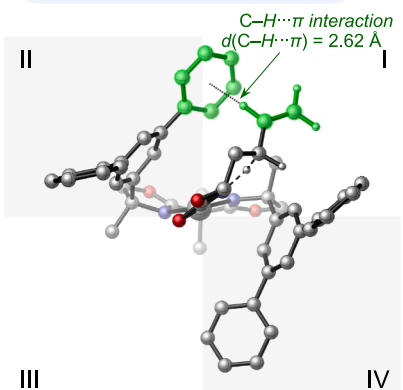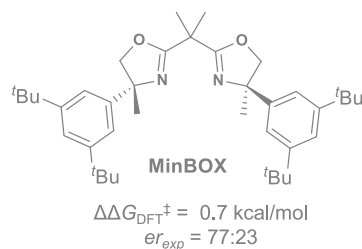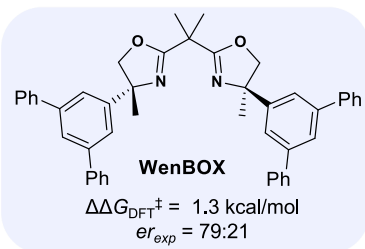With the data from the preliminary ligand screen in hand (Scheme 3C), we turned to optimizing the most promising ligands for each substrate class and expanding the scope. Benzylic amidation of **1a** with (*S,S*)-Min-BOX was conducted using selected other ligands (Scheme 4). The steric impact of (*R,R*)-Wen-BOX **B** compared to (*S,S*)-Min-BOX **A** was highlighted by the need to use a higher loading of **B** to achieve good conversion, although only a slight decrease in *ee* was noted. The use of (*R,R*)-Em-BOX **D** with **1a** gave essentially the same result as the parent ligand. As expected, the bulkier (*R,R*)-naphthyl-BOX **H** resulted in both a decreased yield and *ee*.

We next explored the scope of allylic C–H amidation using selected ligands from Scheme 3C. Amidation of **1b** to **2b** gave a higher 58% *ee* with (*S,S*)-Wen-BOX **B** as compared to (*S,S*)-Min-BOX **A**, while (*R,R*)-Em-BOX **D** further improved the *ee* to 66%, perhaps due to better NCIs between the e-poor alkene and the e-rich aryl ligand group or an increase in steric interactions in the TS leading to the minor enantiomer.[30] As previously described, asymmetric amidation of **19** gave 64% *ee* of **19a** with (*S,S*)-Min-BOX **A**, but the introduction of attractive NCIs via extended conjugation in (*S,S*)-Wen-Box **B** increased the *ee* of **19a** to 72%. The additional rigidity of (*R,R*)-Em-Box **D** improved both yield and *ee* to 82% and 75%, respectively.

Both (*S,S*)-H,H-Min-BOX **I** and (*S,S*)-Cyp-Min-BOX **J** improved the *ee* relative to **A**, suggesting that changes to the bite angle of the ligand may be beneficial. This was explored using (*R,R*)-JAM-BOX **K**, which was hypothesized to have a smaller bite angle compared to **A**. This should enhance C(sp³)–H-π interactions; indeed, **K** gave excellent yield and *ee* for substrates that were problematic for other ligands. Notable examples include an increase in the *ee* of **2b** from 54% with **A** to 94% with **K**, and an increase from 80% *ee* of **24a** with **A** to 91% with **K**.

Computations predicted (Figure 5, bottom) that installing a *trans*-Ph group at the terminal alkene carbon in **22** would improve *ee* as compared to **1b**. This was validated experimentally, with the *ee* of **22a** increasing to 84% as compared to only 54% *ee* in **2b**. As expected, the greater steric demand of the (*S,S*)-Wen-BOX ligand gave decreased yield and *ee* of **22a** to 62% and 72%, respectively, but both yield and *ee* were improved to 86% and 86%, respectively, with (*R,R*)-Em-BOX **D**.

Yields and *ee* of asymmetric amidations of alkenes **23–29**, bearing differing substitution patterns, were examined for trends to help predict the best catalyst for a given substrate. *cis*- or 2,2′-disubstituted alkenes (**23**, **24**) gave poor conversions to the desired **23a** and **24a**, with *ee* values of 32% and 80%, respectively; conversion is easily increased using higher catalyst loadings. In terms of *ee*, computations predicted the addition of a single Ph group *cis* to the carbamate tether in **23** would yield little difference in the energies of the enantiodetermining TS using the (*S,S*)-Wen-BOX **B** (Figure 5, bottom); experimentally, this was validated with a higher 87% yield of **23a** but no *ee*, indicating a lack of NCIs or steric interactions able to differentiate between the enantiotopic TS. Interestingly, the presence of a *trans* substituent on the alkene, whether an aryl (**22**, **25–27**) or alkyl/heteroalkyl (**28**, **29**) group, gave significantly improved yields and good to excellent *ee*. For example, an aryl group at the internal alkene carbon of **25** gave **25a** in 85% yield and 76% *ee*, while moving the phenyl group to the terminal carbon of **26** improved yield and *ee* to 90% and 98%, respectively. Decreasing the size of the group *cis* to the group undergoing amidation from a Ph in **26** to a Me in **27** decreased *ee* in **27a** to 78%. A TBS group in **28** gave **28a** in 94% *ee*, suggesting that steric bulk in the *trans* position is key to high *ee* but is not required to be an aryl group. This fits our computational model (Figure 5, bottom), as increased steric interactions in the conformer leading to the minor enantiomer raises its energy relative to the conformer giving the

*lowest-energy TS conformers of amination of **1b** with Wen-BOX ligand*

WenBOX

$\Delta\Delta G_{DFT}^{\ddagger} = 1.3$ kcal/mol
$er_{exp} = 79{:}21$

MinBOX

$\Delta\Delta G_{DFT}^{\ddagger} = 0.7$ kcal/mol
$er_{exp} = 77{:}23$

C–H···π interaction
$d(C{-}H{\cdots}\pi) = 2.62$ Å

ligand–substrate repulsion

substrate distortion

TS9
$\Delta\Delta G^{\ddagger} = 0.0$ kcal/mol

*leading to the major product (R)-**2b***

TS10
$\Delta\Delta G^{\ddagger} = 1.3$ kcal/mol

*leading to the minor product (S)-**2b***
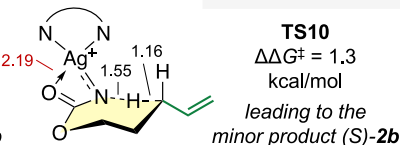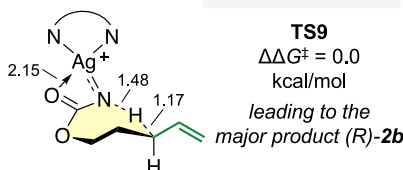
*lowest-energy TS conformers of amination of **19** with Min-BOX ligand*

19
$\Delta\Delta G_{DFT}^{\ddagger} = 2.2$ kcal/mol
$er_{exp} = 92{:}8$

1b
$\Delta\Delta G_{DFT}^{\ddagger} = 0.7$ kcal/mol
$er_{exp} = 77{:}23$

C–H···π interaction
$d(C{-}H{\cdots}\pi) = 2.99$ Å

ligand–substrate repulsion

substrate distortion

TS11
$\Delta\Delta G^{\ddagger} = 0.0$ kcal/mol

*leading to the major product (R)-**19a***

TS12
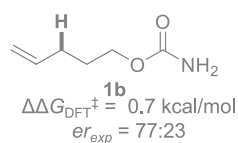$\Delta\Delta G^{\ddagger} = 2.2$ kcal/mol

*leading to the minor product (S)-**19a***
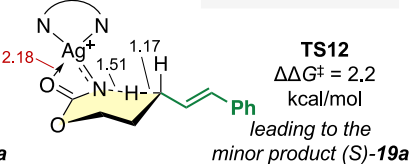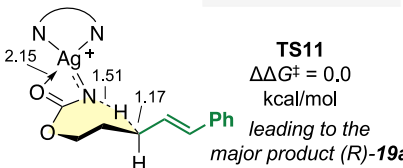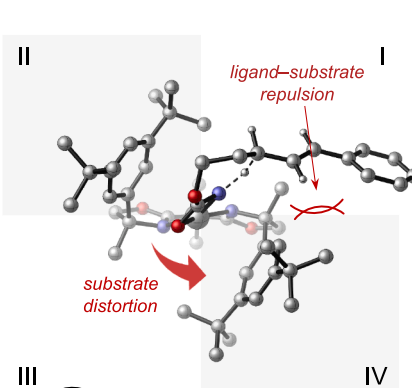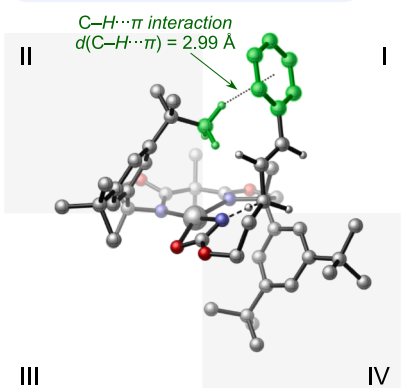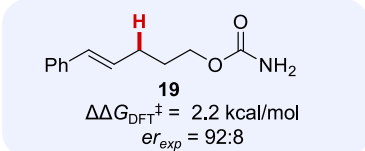
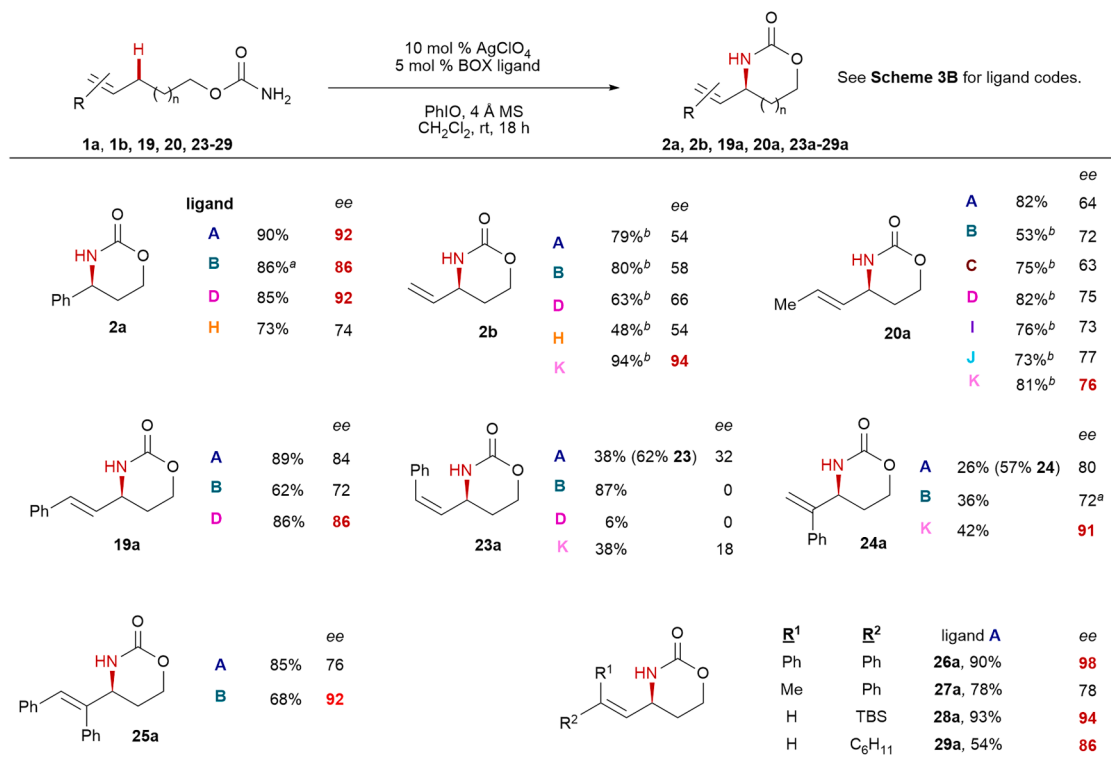**Figure 5. Computationally predicted ligand and substrate effects on the *ee***

Scheme 3. Synthesis and preliminary studies of new ligands for Ag-catalyzed nitrene transfer
(A) New modular synthetic route to (S,S)- and (R,R)-Min-BOX.
(B) Analogs informed by computational studies.
(C) Heatmaps of yield and ee for selected substrates at RT.
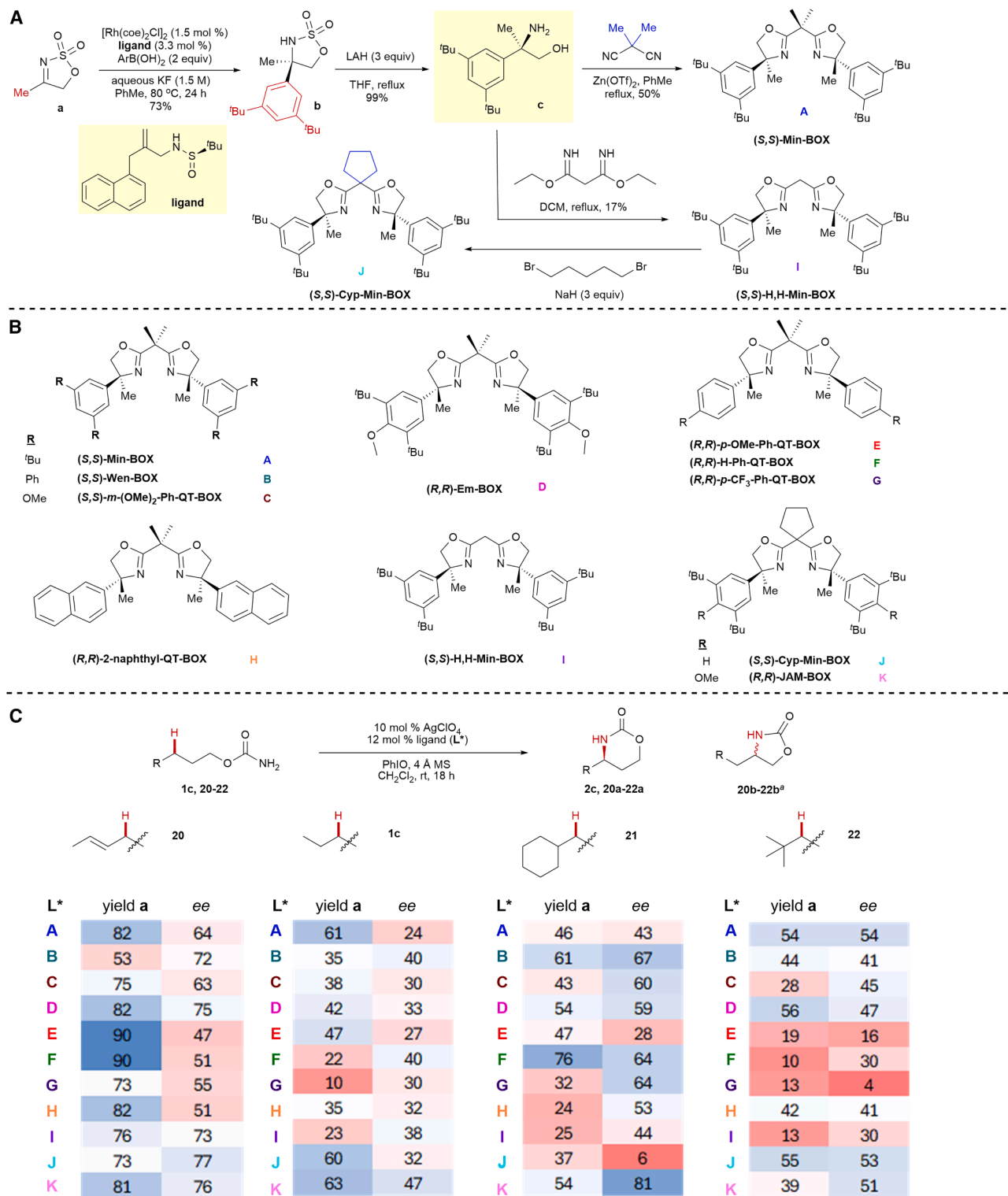
[a] See the supplemental information for details on the competing formation of **b**.

Panel C data:

Substrate 20:

L*	yield a	ee
A	82	64
B	53	72
C	75	63
D	82	75
E	90	47
F	90	51
G	73	55
H	82	51
I	76	73
J	73	77
K	81	76

Substrate 1c:

L*	yield a	ee
A	61	24
B	35	40
C	38	30
D	42	33
E	47	27
F	22	40
G	10	30
H	35	32
I	23	38
J	60	32
K	63	47

Substrate 21:

L*	yield a	ee
A	46	43
B	61	67
C	43	60
D	54	59
E	47	28
F	76	64
G	32	64
H	24	53
I	25	44
J	37	6
K	54	81

Substrate 22:

L*	yield a	ee
A	54	54
B	44	41
C	28	45
D	56	47
E	19	16
F	10	30
G	13	4
H	42	41
I	13	30
J	55	53
K	39	51

Scheme 4. Scope of asymmetric Ag-catalyzed amidation of benzylic and allylic C–H bonds with selected ligands

Reaction conditions: 10 mol % AgClO$_4$, 5 mol % BOX ligand, PhIO, 4 Å MS, CH$_2$Cl$_2$, rt, 18 h. Starting materials **1a, 1b, 19, 20, 23–29** → products **2a, 2b, 19a, 20a, 23a–29a**. See **Scheme 3B** for ligand codes.

2a (Ph)

ligand		ee
A	90%	92
B	86%^{a}	86
D	85%	92
H	73%	74

2b

ligand		ee
A	79%^{b}	54
B	80%^{b}	58
D	63%^{b}	66
H	48%^{b}	54
K	94%^{b}	94

20a (Me)

		ee
A	82%	64
B	53%^{b}	72
C	75%^{b}	63
D	82%^{b}	75
I	76%^{b}	73
J	73%^{b}	77
K	81%^{b}	76

19a (Ph)

		ee
A	89%	84
B	62%	72
D	86%	86

23a (Ph)

		ee
A	38% (62% **23**)	32
B	87%	0
D	6%	0
K	38%	18

24a (Ph)

		ee
A	26% (57% **24**)	80
B	36%	72^a
K	42%	91

25a (Ph, Ph)

		ee
A	85%	76
B	68%	92

R^1	R^2	ligand A	ee
Ph	Ph	**26a**, 90%	98
Me	Ph	**27a**, 78%	78
H	TBS	**28a**, 93%	94
H	C$_6$H$_{11}$	**29a**, 54%	86

^{a} 20 mol % [Ag], 10 mol % **L**, 20 h. ^{b} ee was determined after benzylation.

major enantiomer. Replacing the *trans* H group of **1b** with a cyclohexyl in **29** also improved the *ee* from 54% in **2b** to 86% in **29a**.

To summarize progress in catalyst design for asymmetric amidation of allylic C–H bonds, the presence of an aryl, alkyl, or silyl group in the *trans* position is ideal and gives *ee* up to 98% with ligand **A**. Both 1,1′,2- and 1,2,2′-trisubstituted alkenes are promising, with *ee* up to 98%; ligand **A** is usually sufficient, but *ee* can be improved using our new ligands **B**, **D**, and **K**. A terminal alkene gives 94% *ee* with **K**, while a 2,2′-alkene gives 91% *ee* with **K**. The only class of alkenes that did not furnish high *ee* for the product allylic amine were *cis*-disubstituted alkenes.

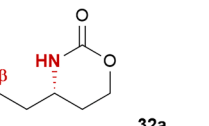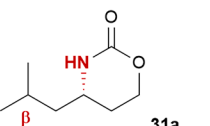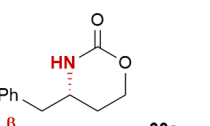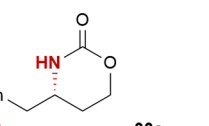### Asymmetric amidation of unactivated C–H bonds
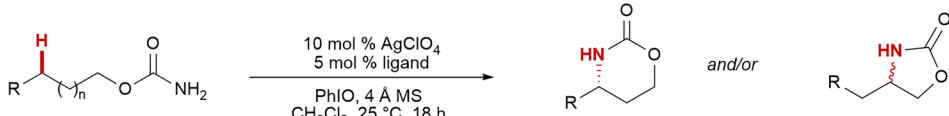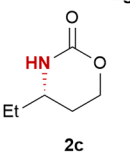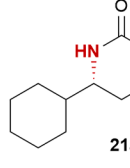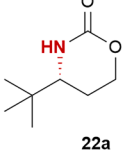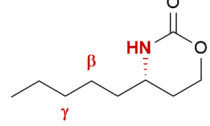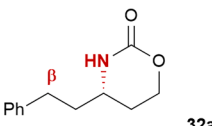
Chemocatalyzed asymmetric amidations of unactivated prochiral C–H bonds to yield enantioenriched 1,3-aminoalcohols are essentially unknown. Some trends were described in Scheme 3C for reaction of **1c** and **21–22**, but we wanted to expand the scope. As shown in Scheme 5, an Et group proximal to the γ site for C–H insertion in **1c** gave only 24% *ee* with (*S,S*)-Min-BOX **A**, which improved to 40% *ee* using (*S,S*)-Wen-BOX **B**. Increasing the length of the linear alkyl group from Et to C$_5$H$_{11}$ in **30** improved the *ee* of **30a** to 58% with (*S,S*)-Min-BOX **A** and to 52% *ee* using (*S,S*)-Wen-BOX **B**. The reduced reactivity of **B**, even at RT, pointed to increased steric demand in **B**, although yield was restored with (*R,R*)-Em-BOX **D**, accompanied

by 66% *ee*. Other carbamates with no branching until the γ carbon, such as **32**, gave results similar to **30**, with ligand **D** furnishing the highest *ee* of 65%.

Substrates with branching at the β sites of **31** and **33** (Scheme 5) did not follow the same trends as observed for **30** and **32**. Nonetheless, *ee* of >50% could be obtained for both substrates with the appropriate ligands (56% *ee* **31a** with ligand **K**; 55% *ee* **33a** with ligand **B**). These are the highest *ee* observed to date for chemocatalyzed NT into unactivated C–H bonds to form precursors to 1,3-aminoalcohols. These results highlight the challenges associated with predicting the response of substituents of varying steric bulk to changes in the ligand. However, our library of new BOX ligands, combined with computational insights into the major interactions in the transition states that control for site- and enantioselectivity, provides valuable insight for the design of second-generation ligands moving forward.

The utility of the asymmetric NT was demonstrated in a short synthesis of the drug dapoxetine (Scheme 6).[17] The ability to access (*R,R*)-Min-BOX (Scheme 3A) enabled preparation of the desired (*S*)-enantiomer of **2a**. After recrystallization of (*S*)-**2a** to improve the *ee* to 99%, the carbamate ring was hydrolyzed with NaOH. The free amino alcohol product was carried forward without purification and subjected to Eschweiler-Clarke reaction conditions. Finally, dapoxetine was synthesized in 48% overall yield and 90% *ee* via a S$_N$Ar reaction of the methylated amino alcohol with 1-fluoronaphthalene.

Scheme 5. Scope of asymmetric Ag-catalyzed amidation of unactivated C(sp3)–H bonds

DISCUSSION

Our interest in the development of general chemocatalysts for the enantioselective amidation of diverse C–H bonds was explored in this work. We have developed a suite of new ligands for asymmetric Ag-catalyzed NT into diverse C–H bonds to furnish 1,3-aminoalcohol building blocks with high *ee*). Our work highlights the power of integrating experimental and computational approaches in the design of novel BOX ligands tailored to give high *ee* in NT across a range of challenging C–H bonds. For example, we achieved good to excellent *ee* for benzylic amidations of both electron-rich and electron-poor aromatic rings, high *ee* and *dr* in desymmetrizations of benzylic C–H bonds, and the ability to override inherent substrate bias to furnish enantioenriched 1,3-*anti*-aminoalcohols not accessible with other known catalysts.

Computational insights showed that a combination of ligand-induced substrate distortion and stabilizing C–H/π interactions between the chiral ligand and the substrate in the TS influences enantioinduction. Computed TS structures with substrates yielding low *ee* exhibited weaker dispersion interactions, diminished stabilizing effects, or smaller steric-induced Ag-nitrene distortions, ultimately resulting in ineffective enantiodiscrimination. These studies provided us with a roadmap to develop improved ligands for asymmetric amidation of allylic C–H and unactivated alkyl C(sp3)–H bonds by fine-tuning steric interactions and NCIs in the enantiodetermining TS. The utility of this

chemistry was demonstrated in a short synthesis of the drug dapoxetine. Ultimately, the melding of experimental and detailed computational studies underscored the importance of subtle effects on *ee*, paving the way for predictive designs of next-generation Ag catalysts for asymmetric NT.

METHODS

Synthesis of compound 2a
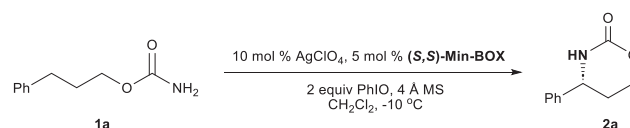
A pre-dried 16 × 100-mm glass test tube equipped with a magnetic stir bar was charged with AgClO$_4$ (4.2 mg, 20 μmol, 10 mol %), (*S,S*)-Min-BOX ligand (5.9 mg, 10 μmol, 5 mol %), and dry CH$_2$Cl$_2$ (4 mL). The test tube was capped with a rubber septum and the reaction mixture was stirred vigorously for 15 min at RT. Powdered 4-Å molecular sieves (200 mg, 1 g of sieves/mmol of substrate) were added, followed by the carbamate ester substrate **1a** (0.2 mmol, 1.0 equiv). After adjusting the reaction temperature to −10°C using a chiller, iodosobenzene (88 mg, 0.4 mmol, 2.0 equiv) was added in one portion and the reaction mixture was stirred at −10°C for 48 h. The mixture was filtered through a pad of Celite rinsing with EtOAc, and the filtrate
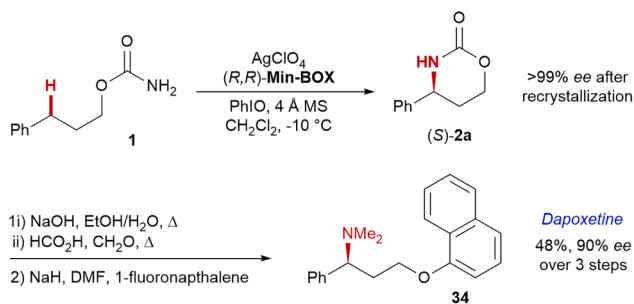
Scheme 6. Application of asymmetric benzylic C–H amidation to a short synthesis of dapoxetine

concentrated under reduced pressure. Silica gel column chromatography (0%→100% EtOAc/hexanes) afforded the oxazinanone **2a** as a white solid (31.9 mg, 90% yield).

TLC: R$_f$ = 0.24 in 80% EtOAc/hexanes.

^1H *NMR*: (500 MHz, CDCl$_3$) δ 7.45–7.37 (m, 2H), 7.37–7.29 (m, 3H), 5.27 (s, 1H), 4.71–4.62 (m, 1H), 4.37–4.27 (m, 2H), 2.32–2.21 (m, 1H), 2.05–1.95 (m, 1H).

^{13}C *NMR*: (126 MHz, CDCl$_3$) δ 153.8, 141.2, 129.2, 128.6, 126.1, 65.2, 55.3, 30.7.

HRMS (ESI) *m/z* calcd. for C$_{10}$H$_{11}$NO$_2$ [M + Na]$^+$, 200.0682; found, 200.0681.

The synthesis of other previously reported small molecules can be found in the supplemental information. Details of general synthetic procedures and compound characterization (including tabulated NMR data, high-resolution mass-spectrometry data) are found in the supplemental information. The supplemental information includes Scheme S1, Figures S1–S3, Data S1 (Cartesian coordinates and energies for all computed structures) and Data S2 (HPLC traces for assessing *ee*), and Table S1. Data S3, consisting of copies of the NMR chromatograms, is also available as part of the supplemental information.

RESOURCE AVAILABILITY

Lead contact
Further information and requests for resources should be directed to and will be fulfilled by the lead contact, Jennifer M. Schomaker (schomakerj@chem.wisc.edu).

Materials availability
All materials generated in this study are available from the lead contact without restriction.

Data and code availability
The datasets generated during this study are available in the supplemental information.

AUTHOR CONTRIBUTIONS

J.M.S., E.Z.S., and J.H.K. designed the experiments and wrote the paper. P.L. and Y.F. designed the DFT studies and wrote the paper. E.Z.S., J.H.K., and W.L. conducted the experiments. Y.F. performed the DFT calculations.

DECLARATION OF INTERESTS

The authors declare no competing interests.

REFERENCES

1. Heravi, M.M., and Zadsirjan, V. (2020). Prescribed Drugs Containing Nitrogen Heterocycles: An Overview. RSC Adv. *10*, 44247–44311. https://doi.org/10.1039/D0RA09198G.

2. Ricci, A. (2008). Amino Group Chemistry: From Synthesis to the Life Sciences (Wiley).

3. Collet, F., Lescot, C., and Dauban, P. (2011). Catalytic C-H Amination: The Stereoselectivity Issue. Chem. Soc. Rev. *40*, 1926–1936. https://doi.org/10.1039/C0CS00095G.

4. Uchida, T., and Hayashi, H. (2020). Recent Development in Asymmetric C-H Amination via Nitrene Transfer Reactions. Eur. J. Org. Chem. *8*, 909–916. https://doi.org/10.1002/ejoc.201901562.

5. Ju, M., and Schomaker, J.M. (2021). Nitrene Transfer Catalysts for Enantioselective C–N Bond Formation. Nat. Rev. Chem *5*, 580–594. https://doi.org/10.1038/s41570-021-00291-4.

6. Park, Y., and Chang, S. (2019). Asymmetric Formation of γ-Lactams via C–H Amination Enabled by Chiral Hydrogen-Bond-Donor Catalysts. Nat. Catal. *2*, 219–227. https://doi.org/10.1038/s41929-019-0230-x.

7. Xing, Q., Chan, C.M., Yeung, Y.W., and Yu, W.Y. (2019). Ruthenium(II)-Catalyzed Enantioselective γ-Lactams Formation by Intramolecular C-H Amination of 1,4,2-Dioxazol-5-Ones. J. Am. Chem. Soc. *141*, 3849–3853. https://doi.org/10.1021/jacs.9b00535.

8. Li, C., Lang, K., Lu, H., Hu, Y., Cui, X., Wojtas, L., and Zhang, X.P. (2018). Catalytic Radical Process for Enantioselective Amination of C(Sp³)−H Bonds. Angew. Chem. Int. Ed. *57*, 16837–16841. https://doi.org/10.1002/anie.201808923.

9. Lang, K., Torker, S., Wojtas, L., and Zhang, X.P. (2019). Asymmetric Induction and Enantiodivergence in Catalytic Radical C-H Amination via Enantiodifferentiative H-Atom Abstraction and Stereoretentive Radical Substitution. J. Am. Chem. Soc. *141*, 12388–12396. https://doi.org/10.1021/jacs.9b05850.

10. Lang, K., Li, C., Kim, I., and Zhang, X.P. (2020). Enantioconvergent Amination of Racemic Tertiary C–H Bonds. J. Am. Chem. Soc. *142*, 20902–20911. https://doi.org/10.1021/jacs.0c11103.

11. Yang, Y., Cho, I., Qi, X., Liu, P., and Arnold, F.H. (2019). An Enzymatic Platform for the Asymmetric Amination of Primary, Secondary and Tertiary C (sp³)–H Bonds. Nat. Chem. *11*, 987–993. https://doi.org/10.1038/s41557-019-0343-5.

12. Nasrallah, A., Lazib, Y., Boquet, V., Darses, B., and Dauban, P. (2020). Catalytic Intermolecular C(sp³)-H Amination with Sulfamates for the Asymmetric Synthesis of Amines. Org. Process Res. Dev. *24*, 724–728. https://doi.org/10.1021/acs.oprd.9b00424.

13. Zalatan, D.N., and Du Bois, J. (2008). A chiral rhodium carboxamidate catalyst for enantioselective C-H amination. J. Am. Chem. Soc. *130*, 9220–9221. https://doi.org/10.1021/ja8031955.

14. Milczek, E., Boudet, N., and Blakey, S. (2008). Enantioselective C-H Amination Using Cationic Ruthenium(II)-Pybox Catalysts. Angew. Chem. Int. Ed. *47*, 6825–6828. https://doi.org/10.1002/anie.200801445.

15. Reddy, R.P., and Davies, H.M.L. (2006). Dirhodium tetracarboxylates derived from adamantylglycine as chiral catalysts for enantioselective C-H aminations. Org. Lett. *8*, 5013–5016. https://doi.org/10.1021/ol061742l.

16. Zhou, Z., Tan, Y., Shen, X., Ivlev, S., and Meggers, E. (2021). Catalytic Enantioselective Synthesis of β-Amino Alcohols by Nitrene Insertion. Sci. China Chem. *64*, 452–458. https://doi.org/10.1007/s11426-020-9906-x.

17. Modi, N.B., Dresser, M.J., Simon, M., Lin, D., Desai, D., and Gupta, S. (2006). Single- and Multiple-Dose Pharmacokinetics of Dapoxetine Hydrochloride, a Novel Agent for the Treatment of Premature Ejaculation. J. Clin. Pharmacol. *46*, 301–309. https://doi.org/10.1177/0091270005284850.

18. Lang, L., Lam, T., Chen, A., Jensen, C., Duncan, L., Kong, F.C., Kurago, Z. B., Shay, C., and Teng, Y. (2020). Circumventing AKT-Associated Radioresistance in Oral Cancer by Novel Nanoparticle-Encapsulated Capivasertib. Cells *9*, 533. https://doi.org/10.3390/cells9030533.

19. Yan, L., Huo, P., Debenham, J.S., Madsen-Duggan, C.B., Lao, J., Chen, R. Z., Xiao, J.C., Shen, C.–P., Stribling, D.S., Shearman, L.P., et al. (2010). Discovery of N-[(4R)-6-(4-Chlorophenyl)-7-(2,4-dichlorophenyl)-2,2-dimethyl-3,4-dihydro-2H-pyrano[2,3-b]pyridin-4-yl]-5-methyl-1H-pyrazole-3-carboxamide (MK-5596) as a Novel Cannabinoid-1 Receptor (CB1R) Inverse Agonist for the Treatment of Obesity. J. Med. Chem. *53*, 4028–4037. https://doi.org/10.1021/jm100023j.

20. Ju, M., Zerull, E.E., Roberts, J.M., Huang, M., Guzei, I.A., and Schomaker, J.M. (2020). Silver-Catalyzed Enantioselective Propargylic C–H Bond Amination through Rational Ligand Design. J. Am. Chem. Soc. *142*, 12930–12936. https://doi.org/10.1021/jacs.0c05726.

21. Watkins, A.L., Hashiguchi, B.G., and Landis, C.R. (2008). Highly enantioselective hydroformylation of aryl alkenes with diazaphospholane ligands. Org. Lett. *10*, 4553–4556. https://doi.org/10.1021/ol801723a.

22. Liu, M.-Q., Jiang, T., Chen, W.-W., and Xu, M.-H. (2017). Highly enantioselective Rh/chiral sulfur-olefin-catalyzed arylation of alkyl-substituted non-benzofused cyclic N-sulfonyl ketimines. Org. Chem. Front. *4*, 2159–2162. https://doi.org/10.1039/C7QO00555E.

23. DFT calculations were performed at the ωB97X-D/def2-TZVPP/CPCM (DCM)//ωB97X-D/def2-TZVPP(Ag)–def2-SVP level of theory.

24. Ma, Q., and Werner, H.-J. (2019). Accurate Intermolecular Interaction Energies Using Explicitly Correlated Local Coupled Cluster Methods [PNO-LCCSD(T)-F12]. J. Chem. Theory Comput. *15*, 1044–1052. https://doi.org/10.1021/acs.jctc.8b01098.

25. Ma, Q., and Werner, H.J. (2021). Scalable Electron Correlation Methods. 8. Explicitly Correlated Open-Shell Coupled-Cluster with Pair Natural Orbitals PNO-RCCSD(T)-F12 and PNO-UCCSD(T)-F12. J. Chem. Theory Comput. *17*, 902–926. https://doi.org/10.1021/acs.jctc.0c01129.

26. Fu, Y., Zerull, E.E., Schomaker, J.M., and Liu, P. (2022). Origins of catalyst-controlled selectivity in the Ag-catalyzed regiodivergent C-H amination. J. Am. Chem. Soc. *144*, 2735–2746. https://doi.org/10.1021/jacs.1c12111.

27. Dolan, N.S., Scamp, R.J., Yang, T., Berry, J.F., and Schomaker, J.M. (2016). Catalyst-controlled and tunable, chemoselective silver-catalyzed intermolecular nitrene transfer: experimental and computational studies. J. Am. Chem. Soc. *138*, 14658–14667. https://doi.org/10.1021/jacs.6b07981.

28. Huang, M., Yang, T., Paretsky, J.D., Berry, J.F., and Schomaker, J.M. (2017). Inverting steric effects: using "attractive" noncovalent interactions to direct silver-catalyzed nitrene transfer. J. Am. Chem. Soc. *139*, 17376–17386. https://doi.org/10.1021/jacs.7b07619.

29. Weatherly, C., Alderson, J.M., Berry, J.F., Hein, J.E., and Schomaker, J.M. (2017). Catalyst-controlled nitrene transfer by tuning metal:ligand ratios: insight into the mechanisms of chemoselectivity. Organometallics *36*, 1649–1661. https://doi.org/10.1021/acs.organomet.7b00190.

30. Motloch, P., Jašík, J., and Roithová, J. (2021). Gold(I) and silver(I) π--complexes with unsaturated hydrocarbons. Organometallics *40*, 1492–1502. https://doi.org/10.1021/acs.organomet.1c00143.